OMAE2018-78753

CALIBRATION OF A TIME-DOMAIN NUMERICAL HYDRODYNAMIC MODEL FOR MOORING ANALYSIS OF A SEMI-SUBMERSIBLE

Nuno Fonseca
SINTEF Ocean
Trondheim, Norway
nuno.fonseca@sintef.no

Carl Trygve Stansberg
Ctstansberg Marinteknikk
Trondheim, Norway
ctstansberg.marinteknikk@gmail.com

ABSTRACT

The paper presents calibration of a time domain numerical model for the motions of the Exwave Semi in high seastates with current. The time domain equations of motion combine linear radiation, linear diffraction and second order wave drift forces, based on MULDIF diffraction code, with nonlinear forces from quadratic damping and from the mooring system. Calibration is performed by comparing simulations with model test data and adjusting hydrodynamic coefficients known to be affected by uncertainty. These include wave drift force coefficients, damping and added mass coefficients. Correction of the drift coefficients is based on empirical quadratic transfer functions (QTFs) identified from the test data by a nonlinear data analysis technique known as "cross-bi-spectral analysis".

Initial "uncalibrated" numerical models are based on input from the mooring, vessel mass, MULDIF hydrodynamic analysis, decay tests and current coefficients. They need adjustments for surge and sway. Empirical drift coefficients, natural periods and damping coefficients are then adjusted by matching low frequency surge and sway spectra. Wave-frequency coefficients need no adjustment. Low frequency wave drift forces, damping and added mass need increase in high sea states, in particular with current. Final motion simulations show 30% - 40% underestimation in initial simulations, while final calibrated simulations are close to the measured records.

1 INTRODUCTION

The EXWAVE Joint Industry Project (EXWAVE JIP - Wave forces on floating units in extreme seas) objective was to investigate extreme wave forces on floating units which may lead to overloading of mooring line, with emphasis on slowly varying wave exciting forces and related low frequency motions (Fonseca et al. 2016, 2017). The motivation to initiate the JIP was the considerable number of incidents with mooring line failures reported until around 2015 – see for example Kvitrud (2014).

It is acknowledged that standard calculations methods based on potential flow theory lead to underestimation of the wave drift forces on Semi submersibles in high seastates (Stansberg 2015, Aksnes et al. 2015, Fonseca and Stansberg 2017a). The main reason is related to viscous drift which is not considered by potential flow methods. A similar tendency, although less pronounced, has been observed also for FPSOs under certain seastate conditions (Fonseca and Stansberg 2017b). The low frequency excitation works together with the low frequency damping to govern the motion response. There is in fact a large uncertainty in the estimation of the low frequency damping, especially in high seastates. For these reasons, the need for calibration of numerical models for mooring analysis, based on model test data, has been pointed out before, as for example by Aksnes et al. (2014, 2015) and Babak et al. (2015).

Two floating units were selected for the EXWAVE investigations, namely a Semi-submersible and a Floating Productions Storage and Offloading vessel (FPSO). This paper deals with the Semi-submersible. More specifically, it describes the numerical model implemented for the horizontal moored floating structure, its calibration and comparison with model test data. The focus is mainly on high sea states relevant for design analysis. The numerical model is implemented in SIMO (Ormberg et al. 2013), which can be considered a state of the art time domain code to calculate the nonlinear motion responses of floating moored systems.

2 CASE STUDY

2.1 Model tests

Model tests were performed at the Ocean Basin Facility at MARINTEK during October 2015 with a 1:50 scaled model of the Exwave semi-submersible. This platform represents a classical drilling rig with four columns and two pontoons. Figure 1 shows a photo of the model, while Table 1 presents the platform main particulars.

The tests focused on the dynamic behaviour of the platform in waves and current. The aim of the model test program was to obtain test data to: (a) identify the slowly varying wave drift forces and the related slow drift damping and (b) assess the quality of slow drift motions numerical predictions. The focus is on the horizontal low frequency motions induced by severe seastates. The wave-current interaction effects on the wave drift forces are also addressed.
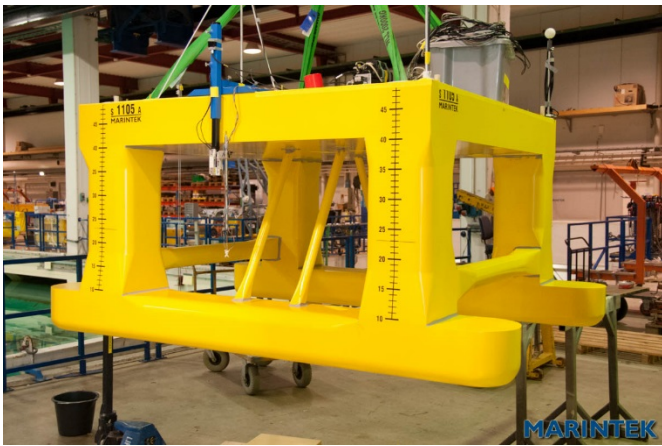

Figure 1: EXWAVE semi-submersible 1:50 scaled model.

Table 1: EXWAVE semi-submersible main properties.

Parameter	Unit	Full scale
Length of pontoons	[m]	107.5
Breadth outside pontoons	[m]	81.25
Width of pontoons	[m]	14.26
Height of pontoons	[m]	9.50
Width of columns	[m]	12.50
Breadth of columns	[m]	12.50
Survival draft	[m]	23.0
Displacement	[t]	39206
Longit. centre of gravity, LCG	[m]	0.0
Vertical centre of gravity, VCG	[m]	23.65
Roll radius of gyration, Rxx	[m]	36.1
Pitch radius of gyration, Ryy	[m]	34.4
Yaw radius of gyration, Rzz	[m]	42.3

The tests were performed at 3 m water depth (150 m full scale), which may be considered as deepwater conditions for most of the wave frequency range of interest. The model was moored with a soft horizontal mooring system with (almost) linear restoring forces in surge and sway. The system is composed of 4 thin lines with horizontal angular separation of 45 degrees. Two lines attach at the model portside and two lines at the starboard side, with the other ends at the Ocean Basin sides. Each line includes a system of springs with designed stiffness.

Parameters such as the wave height and current velocity are changed systematically with the objective of characterizing their influence on the wave drift forces. Both regular and irregular wave conditions were used. System identification tests were performed as well.

2.2 Cases selected for calibration

Four test cases from the test matrix were selected for comparison with numerical simulations and calibration of the numerical model. Table 3 presents the related conditions.

Table 2: Sea state properties corresponding to the selected test cases. Head waves (heading = 0) and collinear waves and current.

Test no.	Wave spectrum	Hs [m]	Tp [s]	Uc [m/s]
4010	Broad band	2.5	5-25	0
4060	Torsethaugen	15.0	16.0	0
4160	Torsethaugen	15.0	16.0	0.82
4260	Torsethaugen	15.0	16.0	1.58

3 CALCULATION AND POST-PROCESSING OF MOTION RESULTS

3.1 SIMA workbench

The vessel motion simulations, the post processing of time signals and comparisons with test data were carried out using the SIMA simulation workbench (SIMA – Simulation and engineering analysis of marine operations and floating systems: https://www.sintef.no/en/software/sima).

3.2 SIMO time domain simulator

The tool for motion calculations is SIMO, a time domain simulation code for nonlinear motions and station keeping analysis of single and multibody systems (Ormberg et al., 2013). The code calculates the vessel's wave frequency and low frequency motion responses induced by wind, waves and current, as well as the corresponding mooring line tensions.

SIMO has two options to calculate the motion responses: by separating the wave frequency (WF) and the low frequency (LF) responses, or by solving them together with one single set of time domain differential equations of motion. The first option was selected for the present work. The WF motions are assumed linear and decoupled from the LF motions, therefore, their time histories are calculated directly from the frequency domain transfer functions. The latter are computed by a linear diffraction/radiation code, as described further ahead in the text. The LF motions are calculated directly in the time domain. The equations of motion may include nonlinear terms, like those arising from the mooring system and risers, quadratic damping forces, forces due to propulsion units, thrusters' forces, couplings between multi-bodies and many other.

Regarding simulation of wave drift forces in irregular waves, they are calculated from mean wave drift force coefficients applying Newman's approximation (Newman, 1974). This is the simpler option in SIMO, which is assumed valid for the present platform moored in deep water.

The mooring system in SIMO is represented by a quasi-static approach, which neglects the lines' dynamic effects. The approach is valid for representation of the present horizontal mooring system. When the mooring system and risers' dynamics need to be considered, SIMO is coupled to RIFLEX, a nonlinear time domain code for static and dynamic analysis of slender marine structures based on finite element modelling (SINTEF Ocean, 2016).

4   METHOD OF CALIBRATION

Calibration consists of adjusting the hydrodynamic model with the aim of achieving numerical time series predictions in good agreement with selected model test cases. Verification and calibration of the numerical model can be split into four items:

A) Reproduction of static restoring forces (mooring stiffness).

B) Reproduction of decay tests and check of the natural periods for all 6 DOF. Set the low frequency damping coefficients as those identified from the decay tests.

C) Check of wave frequency responses and adjust damping coefficients if needed.

D) Drift force coefficients are calibrated by use of estimates from cross-bi-spectral analysis of the test data. The low frequency damping is calibrated for good agreement of LF spectra.

Items A and B comprise the following steps:

1) Numerical and experimental static pull-outs are compared. The results must be very close. If needed, the mooring system properties identified during the test campaign may be very slightly fine-tuned.

2) The numerical natural periods of surge, sway and yaw are checked against test data, first comparing decay tests and second comparing resonant periods on the response spectra corresponding to irregular waves. The first must show very comparison with test data without tuning. The natural periods in irregular waves may need to be tuned.

3) The natural periods of free roll and pitch are checked. If needed, the moments of inertia and/or hydrostatic restoring coefficients may be slightly adjusted, but only within the margins of the uncertainty in the model properties identification.

4) The natural periods of roll and pitch for the moored vessel are checked.

5) Simulations of the free decay tests are performed and the results compared directly with the test signals. The numerical model uses the linear and quadratic damping coefficients estimated from the decay tests for surge, sway, roll and pitch.

The numerical model at the end of the previous steps is named here as "Un-calibrated numerical model".

The second part consists of calibration and validation of the wave frequency motions and of the low frequency motions (items C and D). Wave frequency responses may require additional damping to achieve realistic motion amplitudes around the natural frequency. Regarding the low frequency motions, the present paper focus on the surge and sway modes. Usually, the potential flow wave drift

coefficients need to be corrected and the low frequency damping needs to be increased.

The calibration process includes:

6) Simulations for some tested conditions and comparison of the wave frequency motion spectra with corresponding test results. Damping is added if needed.

7) Identification of wave drift force coefficients applying a cross bi spectral analysis to the model test data. Use the result to correct the potential flow drift coefficients.

8) Calibrate the linear and quadratic low frequency damping coefficients with the objective of achieving good agreement of low frequency spectra from measurements and simulations.

The final numerical model is named "Calibrated numerical model".

5   UN-CALIBRATED NUMERICAL MODEL

5.1 Potential flow hydrodynamic coefficients

MULDIF, a three-dimensional linear radiation/diffraction code (Hermundstad et al. 2016), was applied to calculate potential flow hydrodynamic coefficients, linear wave exciting force coefficients and mean wave drift force coefficients. The underwater hull corresponding to the survival draft was modelled by 8956 flat panels. The largest element diagonal is 2.3 m. Figure 2 shows the panel model.
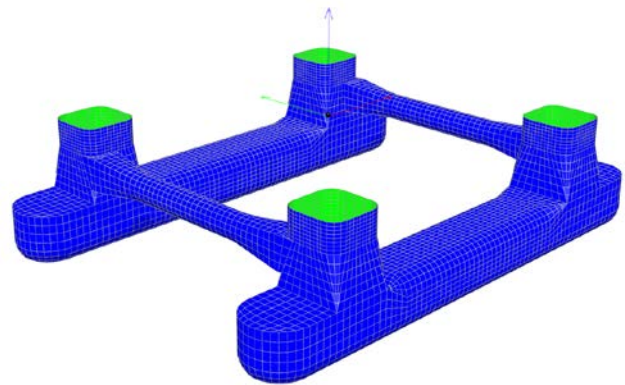

Figure 2: Hull mesh for MULDIF hydrodynamic calculations.

The wave drift damping effects and the wave-current interaction effects on the wave drift forces, $F_i^c(t)$, are represented by one frequency independent coefficient, c_{wd}, which represent a modification of the zero current wave drift forces, $F_i(t)$:

$$F_i^c(t) = F_i(t)\big(1 + c_{wd_i} v_i\big), \qquad i = 1, 2, 6$$

where v_i is the relative velocity. More details can be found in (Ormberg et al., 2013). Analysis with simplified formulations lead to a correction coefficient c_{wd} of 0.25 s/m, which is the value adopted here.

It is acknowledged that the above method is over simplified. A more consistent approach to account for the wave drift damping effects and/or wave-current interaction effects, based on zero current wave drift coefficients, has been proposed before by Aranha's (1996). Babak et al. (2017) presented a method for direct correction of wave drift forces

in the time domain based on the instantaneous relative velocity, which includes contributions from the current and the low frequency velocity. A few state of the art potential flow codes, such as MULDIF (Hermundstad et al. 2016, 2017), can solve the linear potential flow problem and calculate mean wave drift forces accounting for the wave-current interaction.

5.2 Mooring system restoring force

The horizontal mooring system restrains the vessel heading at a mean position with respect to the incoming waves. It consists of 4 lines connected to the semi-submersible model at one end and attached to the edges of the basin (above water) at the other end. The mooring system forces are calculated in SIMO by the "Shooting method". The mooring lines segments are assumed to form catenaries, which are modelled by the catenary equations. The catenary equations are solved by an iteration method. The numerical model is prepared based on the lines properties identified before the model tests.

Figure 3 compares horizontal restoring forces from three pull out tests, with the predictions by SIMO. The agreement is very good.
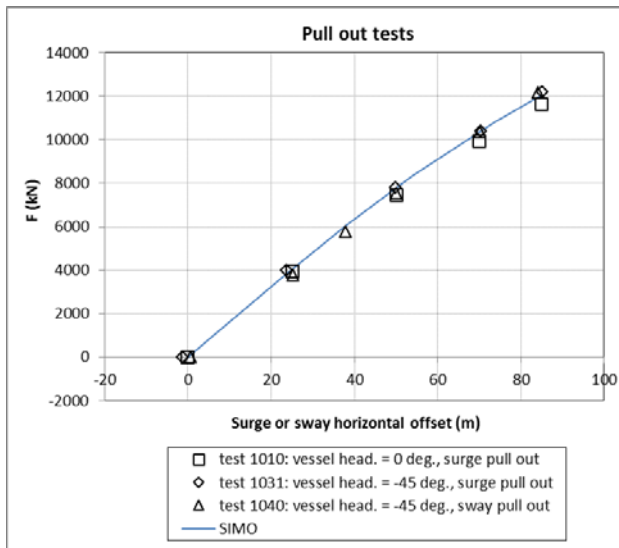

Figure 3: Restoring force as function of the horizontal offset. Results from the pull-out tests and SIMO predictions.

5.3 Verification of natural periods and still water damping

One important check regarding the numerical models is the motions natural periods, since the dynamic behaviour is very much related to this parameter. The following paragraphs present the Exwave Semi natural periods from tests and numerical models.

It is possible to estimate the natural periods from the model test data, namely from the decay tests and from the tests in irregular waves. The second and third columns of Table 2 present results taken from the decay tests without current and from a irregular wave seastate with small significant wave height (Hs). The "irregular waves" periods are not exactly natural periods – these are in fact peak periods from the motions response spectra. In practice, the periods are close to the natural periods for low damping values.

The fourth column includes the peak periods from the MULDIF calculated motion RAOs (RAO – ratio amplitude operator). Finally, the decay tests were reproduced in SIMO and the estimated periods of the free decaying motions presented in the right end column. Overall, there is a good consistency between all the natural periods.

Table 3: Natural periods from model tests (decay tests and and low sea states) and initial numerical models.

Mode	Decay tests	Irreg. wave tests (pink noise)	MULDIF /SIMO RAOs	SIMO Decay
Surge	116.8	122.8	117.6	116.2
Sway	136.1	135.3	-	133.4
Heave	-	22.7	23.1	22.5
Roll	52.1	53.0	52.1	51.0
Pitch	56.6	57.1	57.1	57.0
Yaw	-	80.6	80.0	79.6

6 NUMERICAL MODEL CALIBRATION AND VALIDATION

6.1 Hydrodynamic damping

As explained in Section 3.2, the WF and the LF motions are solved separately. The wave frequency motions are computed in SIMO from the MULDIF motion transfer functions, while the low frequency motions are solved in the time domain.

The effective hydrodynamic damping in MULDIF includes two components:
a) The potential flow radiation damping, which is calculated by MULDIF assuming zero current velocity.
b) Additional linear damping, B_L, which is input to MULDIF through a "Linear damping matrix". The additional damping represents mostly viscous effects and it is used to avoid unrealistic resonance peaks of the motion transfer functions. Heave is the only mode with natural frequency is in the low frequency border of the wave energy band, therefore, in practice, it is the only mode with WF responses being affected by the additional damping. The selected additional damping for the 6 modes varies between 3 and 5 % of the critical damping (see Table 4).

The effective hydrodynamic damping in the present SIMO model for LF motion calculations includes two components:
a) The additional linear damping, B_L, which is input to SIMO through a "Linear damping matrix". Additional linear damping is used for the all six modes of motion. The linear damping for surge, sway, roll and pitch is the one identified from the decay tests. The linear damping in heave and yaw is 3 % and 5 % of the critical damping respectively. Table 4 presents the linear damping values.
b) The additional quadratic damping, B_Q, which is input to SIMO through the "Quadratic damping matrix". Surge, sway, roll and pitch use additional quadratic damping. The roll and pitch quadratic damping coefficients are the ones identified from the decay tests, while the surge and sway ones correspond to the decay tests coefficients, deduced by the quadratic current coefficients (Table 4).

For surge and sway the presented LF damping coefficients are used as a starting point – "initial values" – before final calibration against tests in irregular waves. The final calibration is presented in Section 6.5.

Table 4: Damping coefficients for MULDIF and for the un-calibrated SIMO models.

	Crit. damp. [Ns/m] [Nms]	MULDIF B_L [Ns/m] [Nms]	SIMO B_L [Ns/m] [Nms]	SIMO B_Q [Ns^2/m^2] [Nms^2]
Surge	5.971E+06	2.99E+05	1.39E+05	1.48E+06
Sway	6.826E+06	3.41E+05	-1.71E+04	1.32E+06
Heave	4.314E+07	1.29E+05	1.29E+06	0
Roll	1.904E+10	5.70E+08	5.57E+08	2.71E+10
Pitch	1.700E+10	6.80E+08	5.15E+08	4.94E+10
Yaw	1.759E+10	8.80E+08	8.80E+08	0

Table 4 presents the critical damping coefficient for each degree of freedom, as reference values, together with the additional linear damping applied in MULDIF and the linear and quadratic damping coefficients applied in the un-calibrated SIMO model.

## 6.2 Wave frequency motions

Wave frequency (WF) motions are in general well represented by the numerical model and need not to be calibrated, even for large seastates. This is seen in the example graphs of Figure 4 with wave frequency surge and heave spectra for a small seastates (4010) and a severe seastate (4060). The graphs compare results from model tests (MT), un-calibrated numerical model (Simo potential) and calibrated numerical model (Simo merged_formula). One may consider responses at the wave frequency as those above 0.25 rad/s and below 0.80 rad/s, although the actual range changes with the seastate peak period.

The results show a quite good agreement between motion spectra from model tests and from numerical models. The observation is valid for the small seastate and for the severe seastate, which confirms the hypothesis that the WF motions may be assumed linear.
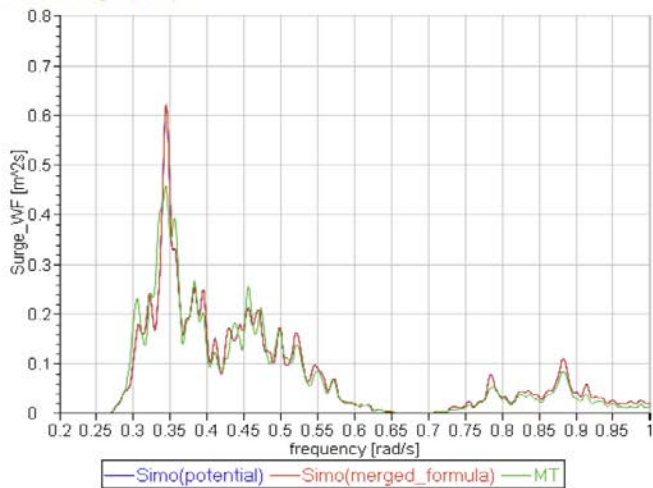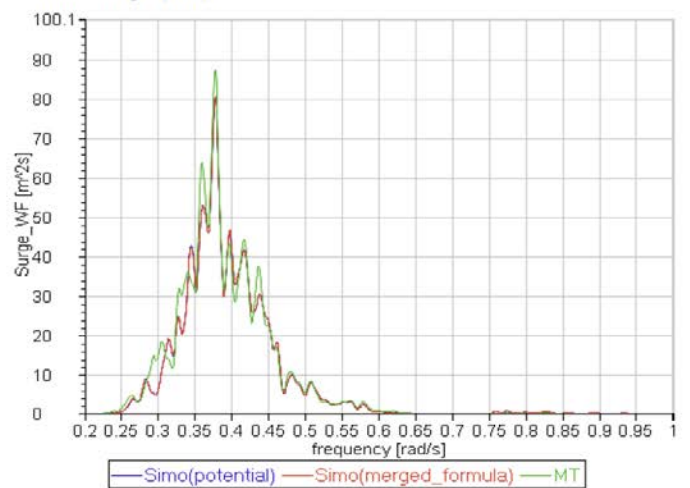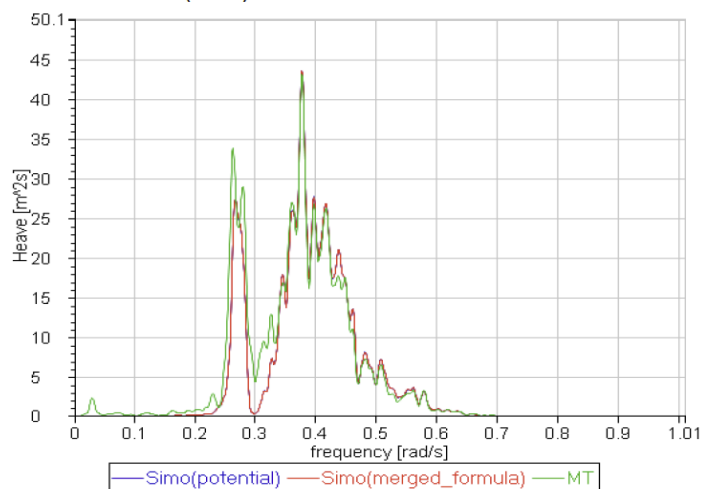

Figure 4: Wave frequency surge spectra (upper graphs) and heave spectra (lower graphs) for seastates 4010 (Hs = 2.5 m, Tp = 5-25 s) and 4060 (Hs = 15 m, Tp = 16 s) under head waves and no current. Comparison between model test results (MT), un-calibrated numerical model (Simo(potential)) and calibrated numerical model (Simo(merged_formula)).

Regarding predictions, the WF responses are the same for the un-calibrated and the calibrated numerical models. This is because variations (calibrations) are introduced only in the low frequency excitation coefficients and horizontal motions damping. These variations not affect the WF motions. The natural frequency of heave is in the lower border of the wave frequency range (0.28 rad/s), therefore the response spectra show resonance peaks. The numerical models are in good agreement with the test results for the severe seastate, but not for the small seastate. This is because the additional damping coefficient was tuned for severe seastates. For the high seastate, there is underestimation of the heave motion for the cancellation frequency (0.3 rad/s), which is related to neglected viscous excitation. Although viscous effects may be computed by MULDIF, in a linearized sense, they have not been included in the present study because the focus is on the low frequency responses.

6.3 Wave drift forces and wave-current interaction effects

The present study follows a method to identify surge wave drift force coefficients from measured vessel responses in irregular waves. A post-processing analysis of the test data is carried out to extract empirical wave drift coefficients making use of a nonlinear data analysis known as "cross-bi-spectral analysis" (CBS) to estimate characteristics of second-order responses represented by Quadratic Transfer Functions – QTFs. Details of the method can be found in Stansberg (1997, 2001) and a summary in Fonseca and Stansberg (2017a).

Figures 5 and 6 present surge wave drift force coefficients in head waves for the seastate with significant wave height (Hs) of 15 m and peak wave period (Tp) of 16 s. The first graph corresponds to conditions without current and the second to conditions with collinear current of 0.82 m/s. The graphs show four lines representing:

- Potential flow mean wave drift force coefficients for zero current.
- Results from the Semi-empirical correction formula as proposed by Stansberg at al. (2015). The correction of potential flow zero current coefficients accounts for viscous effects and wave-current interaction.
- Empirical coefficients identified from the model tests - MT(CBS).
- Corrected results as used by the "calibrated numerical model" and presented in Section 6.5 (Merged). These curves result from merging the empirical coefficients with the "Formula" predictions at the low frequency range and the potential flow coefficients at the high frequency range.

The empirical wave drift coefficients require further explanation. The drift coefficients shown in Figures 5 and 6 correspond to a small constant difference frequency (df). They were extracted from the empirically estimated QTFs. Since the slow drift motion spectra have more energy close to the natural frequency (f_n), the most relevant QTF estimates for actual motions are those at difference frequencies around f_n. The identification is assumed more accurate for the frequency range where the response spectrum has more energy. For this reason, the procedure consists of extracting a

QTF diagonal with df between $df = 0$ and $df = f_n$. In this case $df = 0.0074$ Hz.

Comparing the QTF diagonals described above with mean wave drift force coefficients is valid if the QTF changes slowly around the main diagonal corresponding to $\Delta f = 0$ (which is the same as saying the QTF is nearly constant along diagonals with constant $f_1 + f_2$). This is the case for the EXWAVE Semi.
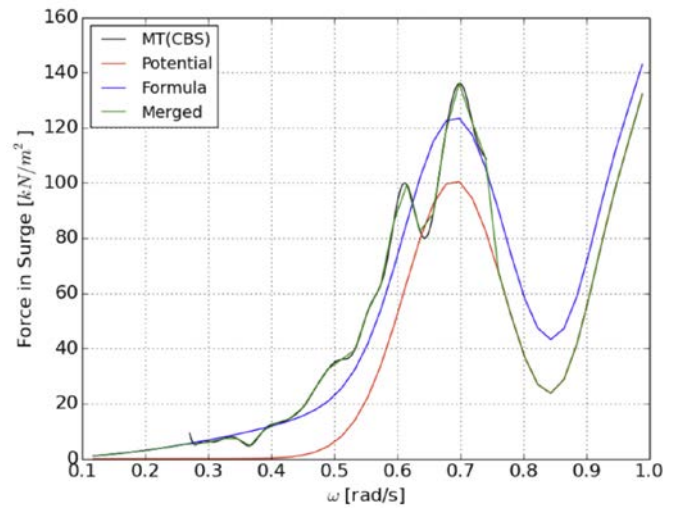
Figure 5: Surge mean wave drift force coefficients for test 4060 (Hs = 15 m, Tp = 16 s, Uc = 0, heading = 0).
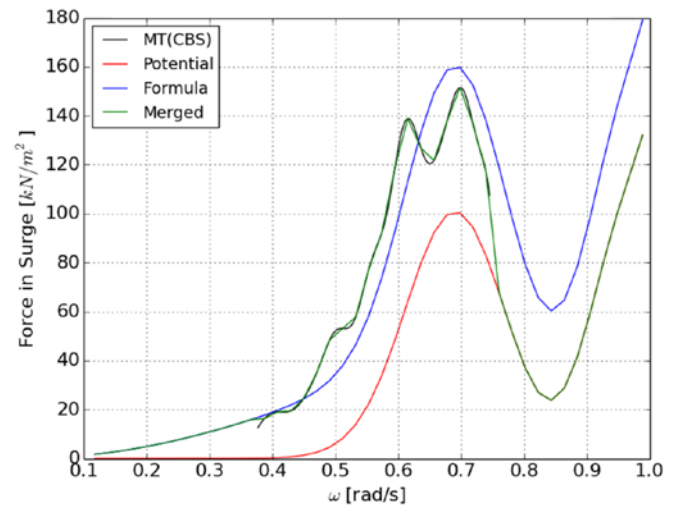
Figure 6: Surge mean wave drift force coefficients for test 4160 (Hs = 15 m, Tp = 16 s, Uc = 0.82 m/s, heading = 0).

As referred, the semi-empirical Formula results were computed according to Stansberg et al. (2015). The Formula was improved during Exwave (Fonseca and Stansberg, 2018).

The results show a large underestimation of the wave drift force coefficients for the frequency range between 0.25 and 0.7 rad/s, as compared to coefficients identified from the model tests. This is exactly the frequency range of the seastate energy (ωp = 0.4 rad/s). Viscous drift is the reason for the discrepancy. Furthermore, the wave drift forces increase for conditions with collinear waves and current. This is due to increased viscous drift effects, while potential flow wave current effects increase the wave drift forces for frequencies above around 0.8 rad/s. Similar observations as

those described above have been reported for other Semis, see for example Larsen et al. (2018) and Fonseca et al. (2018).

6.4 Low frequency surge and calibration of damping and added mass in irregular waves

The initially verified natural periods and damping parameters are given in Tables 3 and 4. It is observed from the model tests in irregular waves that the peak of the surge spectra moves to lower frequencies, especially in long and steep waves. Apparently, the surge natural period increases for severe seastates. This effect can be observed, for example, in the 2nd row of graphs of Figure 7. This Figure presents the LF surge spectra from model tests and from simulations with the un-calibrated and the calibrated numerical models. Comparisons correspond to a small seastate (4010) and three high seastates (Hs = 15 m, Tp = 16 s) with increasing collinear current velocity, namely: 4060 with Uc = 0, 4160 with Uc = 0.82 m/s and 4260 with Uc = 1.58 m/s.

Furthermore, the surge damping also increases with the seastate severity, as compared to the quadratic damping model identified from the calm water tests. Sway LF motion responses show a similar behaviour, however it will not be discussed here.

The full physical explanation for the observations described above is not quite clear, but it is likely related with the increase in viscous effects and, thereby, viscous drift forces. For calibration purposes, we have therefore introduced additional contributions in added mass and damping for the numerical model, obtained by tuning of LF spectra. The result of the tuning for each simulated test is highlighted in Table 5. A_{11}^0 stands for zero frequency surge added mass, B_{11}^L and B_{11}^Q represent the surge linear and quadratic damping coefficients and Cwd is the wave drift damping coefficient.

The SIMO decay test simulation applies the potential flow surge added. The resulting natural period is very close to the experimental one (Table 3). Simulations for the small seastate require a slight increase of the added mass to achieve good agreement of the LF spectra resonance peaks (see Figure 7). Simulations for the large and steep waves require an increase of the added mass of around 60 % of the vessel displacement for conditions without current. The required added mass increase is lower for conditions with current.

Regarding calibration of surge damping, simulations for the small seastate require only a very small increase of the damping, as compared to the decay test value. On the other hand, the severe seastates require a significant increase of the damping to achieve LF spectra comparable to the model tests (Figure 7). The strategy consisted in keeping the linear damping coefficient as identified from the decay test and increase the quadratic damping coefficient.

Note that B_{11}^Q given in the table include effects due to the current coefficient based drag force model as well as additional tuned SIMO values. Finally, one should also note that a small contribution to the LF damping arises from the horizontal mooring system. The four mooring lines used during the model tests are very thin, but were partly beneath the water surface. The related damping effects on the vessel LF motions are assumed small, but in fact not negligible.

The overall conclusion from observation of the graphs of Figure 7 is that the LF numerical model requires almost no calibration for the small seastate, however, for large seastates the un-calibrated simulations largely under-estimate the measured LF motions. The discrepancies increase with the current velocity.

Table 5 requires one note on the values selected for the wave drift damping coefficient, Cwd. A coefficient of 0.25 s/m is applied on numerical model in waves without current, and on numerical models in current using zero-current un-calibrated potential flow drift coefficients. For consistency, it is chosen to be zero when using empirical wave drift coefficients identified from the tests with current, since it would otherwise strictly mean to include wave-current effects on the drift forces twice. In the latter case, the pure net damping effect from the wave drift damping is empirically accounted for through the calibration/tuning procedure.

Table 5: Surge added mass and damping coefficients: potential flow coefficients and calibrated coefficients.

	Hs [m]	Tp [s]	Uc [m/s]	A_{11}^0 [kg]	B_{11}^L [Ns/m]	B_{11}^Q [Ns²/m²]	Cwd [s/m]
MULDIF (Uc = 0)	-	-	-	1.66E+07	0	0	-
SIMO decay test	-	-	-	1.66E+07	1.39E+05	2.15E+06	-
Test 4010	2.5	5-25	0	1.94E+07	1.50E+05	2.15E+06	0.25
Test 4060	15.0	16.0	0	4.00E+07	1.39E+05	4.67E+06	0.25
Test 4160	15.0	16.0	0.82	3.50E+07	1.39E+05	3.87E+06	0
Test 4260	15.0	16.0	1.58	3.00E+07	1.39E+05	3.67E+06	0

Table 6: Statistics of the surge LF motion.

	Test no.	4010	4060	4160	4260
	Hs [m]	2.5	15.0	15.0	15.0
	Tp [s]	5-25	16.0	16.0	16.0
	Uc [m/s]	0	0	0.82	1.58
Mean	Model test	-0.37	-4.90	-10.10	-21.55
	SIMO un-calib.	-0.41	-2.97	-6.65	-15.35
	SIMO calibrated	-0.43	-5.33	-10.16	-19.57
Stdv.	Model test	0.64	3.72	4.15	4.56
	SIMO un-calib.	0.65	2.95	2.50	2.65
	SIMO calibrated	0.67	3.52	4.19	4.47
Max.	Model test	1.62	5.85	-0.05	-9.30
	SIMO un-calib.	1.53	4.65	-0.37	-9.39
	SIMO calibrated	1.58	4.48	-0.49	-9.80
Min.	Model test	-2.76	-24.26	-27.90	-35.10
	SIMO un-calib.	-2.62	-21.32	-17.60	-28.10
	SIMO calibrated	-2.54	-23.25	-24.60	-40.85

The calibrated numerical model spectra compare quite well with the model test data. Calibration required increasing the wave drift force coefficients to account for viscous drift effects, as well as increasing the LF quadratic damping (and also the added mass). It is of interest to highlight that although increasing the drift forces and the damping have contrary effects on the LF motions, the increase of wave drift forces clearly dominate in this respect, since un-calibrated LF surge is significantly lower than the test measurements.
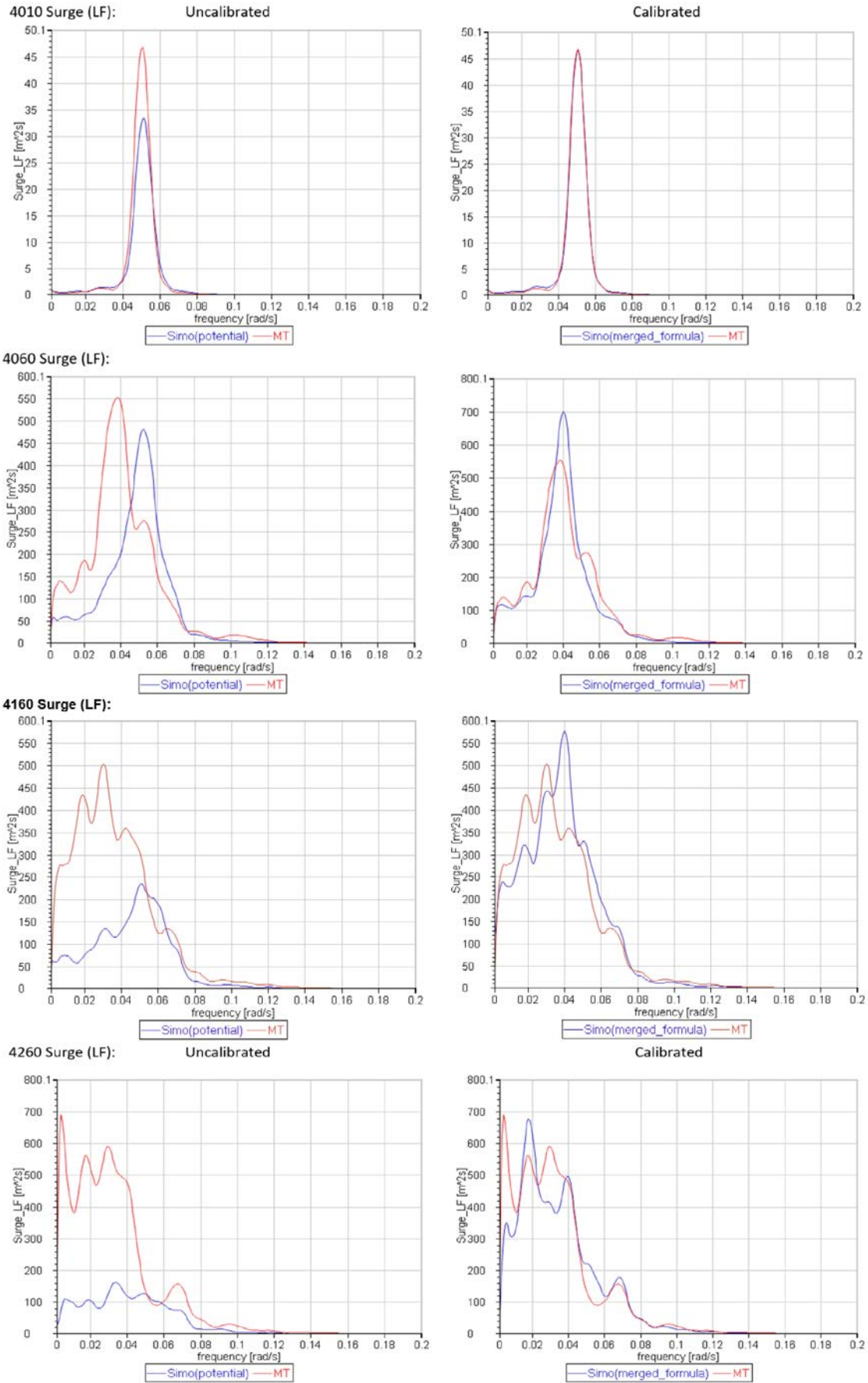
Figure 7: Low frequency surge spectra in head waves for four model tests. Comparison between model test results and predictions from the un-calibrated numerical model (left side) and the calibrated numerical model (right side).
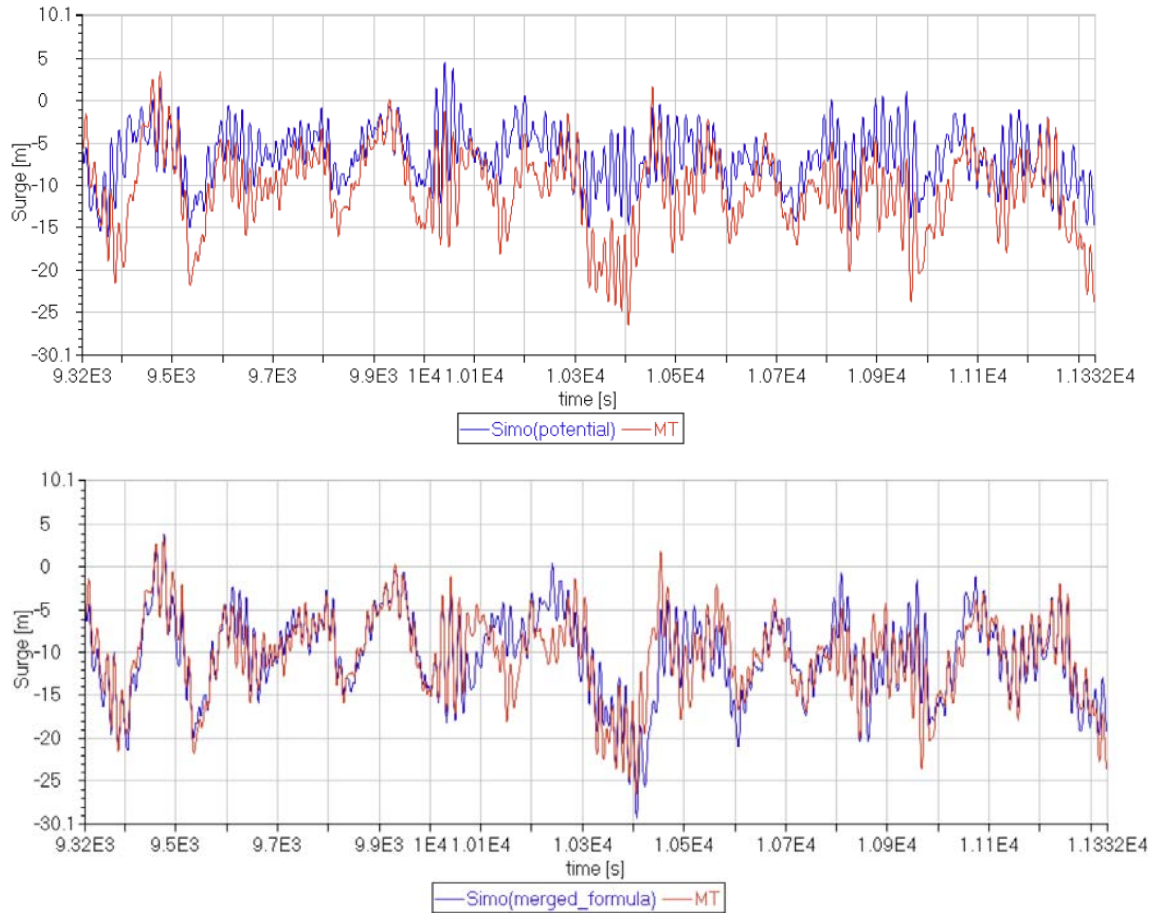
Figure 8: Surge time histories from model tests (red lines) and simulations (blue lines) for test 4160 (Hs = 15 m, Tp = 16 s, collinear Uc = 0.82 m/s). Upper graph with un-calibrated simulations and lower graph with calibrated simulations.

Figure 8 present time histories of the measured and simulated surge motion for a test 4160 (Hs = 15 m, Tp = 16 s, Uc = 0.82 m/s). Un-calibrate predictions on the upper graph and calibrated ones in the lower graph. The better agreement of the calibrated results with the measured motion is obvious. Regarding the un-calibrated results, besides underestimation of the variance, the mean offset is also significantly smaller than the one from measurements.

Finally, Table 6 presents statistics of the LF surge motion. Predictions from the calibrated model for severe seastates compare well with the experiments. Un-calibrated results underestimate the LF standard deviation between 20 % and 40 % and the extreme offsets between 12 % and 38 %.

7   CONCLUSIONS

The paper presents calibration of a time domain numerical model for the motions of the Exwave Semi in high seastates with current. Focus is on the response which introduces the larger uncertainty in the prediction of mooring line tensions, namely the low frequency horizontal motions.

"Un-calibrated" and "calibrated" numerical models are compared with model tests data. The first is validated in terms of mooring system restoring forces and natural period, but otherwise there is no calibration of hydrodynamic coefficients. This model predicts very well the wave frequency motions, even in high seastates. Only the heave motion requires adjustment of the damping coefficient,

because the natural frequency is within the wave frequency range. Regarding the low frequency (LF) surge motion, the un-calibrated predictions are good for the small seastate, but largely underestimate the model tests data, especially for long and steep waves with current. The reason is the neglected viscous effects.

The calibrated numerical model results from adjustment of the LF hydrodynamic coefficients: the wave drift force coefficients, the LF quadratic damping and the surge effective mass need to be increased. The first is estimated by cross bi spectral analysis of the model test data. The second and third are "tuned" to achieve a good agreement between LF motion spectra from tests and from simulations. While the un-calibrated model underestimates the LF motions by 30 – 40 %, the calibrated numerical model results are in good agreement with the tests.

8   ACKNOWLEDGMENTS

9   Copyright © 2018 by ASME

9 REFERENCES

Aksnes, V.Ø., 2014. "Correct" response in positioning analyses. Tekna Conference on DP and Mooring of Floating Structures Offshore, Trondheim, Norway, 12-13 February 2014.

Aksnes, V.Ø., Berthelsen, P.A., Fonseca, N., Reinholdtsen, S-A, 2015. On the need for calibration of numerical models of large floating units against experimental data. The 25th International Offshore and Polar Engineering Conference, Kona, Hawaii Big Island, USA, June 21-26.

Aranha, J.A.P., 1996. Second-order horizontal steady forces and moment on a floating body with small forward speed. *J. Fluid Mech.*, Vol. 313, pp.39-54.

Fonseca, N., Stansberg, C.T., Nestegård, Bøckmann, A., Baarholm, R., 2016. The EXWAVE JIP: Improved procedures to calculate slowly varying wave drift forces on floating units in extreme seas. Proc. of the ASME 2016 35th Int. Conf. on Ocean, Offshore and Arctic Eng., June 19-24, 2016, Busan, South Korea, paper OMAE2016-54829.

Fonseca, N. and Stansberg, C.T., 2017. Wave drift forces and low frequency damping on the Exwave Semi-submersible. Proc. of the ASME 2017 36th Int. Conf. on Ocean, Offshore and Arctic Eng., June 25-30, 2017, Trondheim, Norway, paper OMAE2017-62540.

Fonseca, N. and Stansberg, C.T., 2017. Wave drift forces and low frequency damping on the Exwave FPSO. Proc. of the ASME 2017 36th Int. Conf. on Ocean, Offshore and Arctic Eng., June 25-30, 2017, Trondheim, Norway, paper OMAE2017-62540.

Fonseca, N., Ommani, B., Stansberg, C.T., Bøckmann, A., Birknes-Berg, J., Nestegård, A., de Hauteclocque, G., Baarholm, R., 2017. Wave Forces and Low Frequency Drift Motions in Extreme Seas: Benchmark Studies. Proceedings of the Offshore Technology Conference, paper OTC-27803-MS, 1-4 May 2017, Houston, TX, USA.

Fonseca, N., Stansberg, C.T., Larsen, K., Bjørkli, R., Vigesdal, T., Dalane, O., 2018. Low frequency excitation and damping of four MODUs in severe seastates with current. Proc. of the ASME 2018 37th Int. Conf. on Ocean, Offshore and Arctic Eng., June 17-22, 2018, Madrid, Spain, paper OMAE2018-77873.

Hermundstad, E. M., Hoff, J. R., Stansberg, C. T., and Baarholm, R. J., 2016. "Effects of wave-current interaction on floating bodies". In Proc. 35nd Int. Conf. Ocean, Offshore and Arctic Engineering, OMAE2016, June 19-24, Busan, South Korea.

Kvitrud, A, 2014. Lessons learned from Norwegian anchor line failures 2010-2013. Paper OMAE2014-23095, Proc. OMAE2014, San Francisco, Cal., USA, June 2014.

Larsen, K., Bjørkli, R., Vigesdal, T., Dalane, O., 2018. Mooring of semi submersibles in extreme seastates – simplified models for wave drift forces and low frequency damping. Proc. of the ASME 2018 37th Int. Conf. on Ocean, Offshore and Arctic Eng., June 17-22, 2018, Madrid, Spain, paper OMAE2018-77178.

Ommani, B., Lie, H., Aksnes, V.Ø., Fonseca, N., Berthelsen, P.A., Reinholdtsen, S-A, 2015. Extreme wave loads on Semi-submersible platform columns – a case study. Proceedings of Structural Load and Fatigue on Floating Structures, RINA 2015, February 25, London, UK.

Ommani, B., Fonseca, N. and Stansberg, C.T., 2017. Simulation of low frequency motions in severe seastates accounting for wave-current interaction effects. Proc. of the ASME 2017 36th Int. Conf. on Ocean, Offshore and Arctic Eng., June 25-30, 2017, Trondheim, Norway, paper OMAE2017-62550.

Ormberg, H. et al., 2013. SIMO Theory Manual Version 4.0, rev.3. MARINTEK report no. 516412.00.03.

Newman N., 1974. Second-order, slowly-varying forces on vessels in irregular waves. Proc. Symp. on the Dynamics of Marine Vehicles and Structures in Waves, London, UK, 182-186, April 1974.

SINTEF Ocean, 2016. RIFLEX 4.8.0 user manual.

Stansberg, C.T., 1997. Linear and nonlinear system identification in model testing. *International Conference on Nonlinear Aspects of Physical Model Tests*, OTRC, Texas A&M University, College Station, Texas, 2-3 May 1997.

Stansberg, C.T. 2001. Data Interpretation and System Identification in Hydrodynamic Model Testing. *Proc of 11th Int. Offshore and Polar Eng. Conf., ISOPE,* Stavanger, Norway.

Stansberg, C.T., Kaasen, K.E., Abrahamsen, B.C., Nestgård, A., Shao, Y., Larsen, K., 2015. Challenges in Wave Force Modelling for Mooring Design in High Seas. *Proceedings of the Offshore Technology Conference*, paper OTC-25944-MS, 4-7 May 2015, Houston, TX, USA.

Yang, L., Falkenberg, E., Nestegård, A., Birknes-Berg, J. and Fonseca, N., 2017. Viscous Drift Force and Motions Analysis of Semi-Submersible in Storm Sea States Compared with Model Tests. Proc. of the ASME 2017 36th Int. Conf. on Ocean, Offshore and Arctic Eng., June 25-30, 2017, Trondheim, Norway, paper OMAE2017-62319.